AJNR

Differentiation of Skull Base Chondrosarcomas, Chordomas, and Metastases: Utility of DWI and Dynamic Contrast-Enhanced Perfusion MR Imaging

Y. Ota, E. Liao, A.A. Capizzano, A. Baba, R. Kurokawa, M. Kurokawa and A. Srinivasan

AJNR Am J Neuroradiol published online 11 August 2022
http://www.ajnr.org/content/early/2022/08/11/ajnr.A7607

Published August 11, 2022 as 10.3174/ajnr.A7607

Differentiation of Skull Base Chondrosarcomas, Chordomas, and Metastases: Utility of DWI and Dynamic Contrast-Enhanced Perfusion MR Imaging

Y. Ota, E. Liao, A.A. Capizzano, A. Baba, R. Kurokawa, M. Kurokawa, and A. Srinivasan

ABSTRACT

BACKGROUND AND PURPOSE: Differentiation of skull base tumors, including chondrosarcomas, chordomas, and metastases, on conventional imaging remains a challenge. We aimed to test the utility of DWI and dynamic contrast-enhanced MR imaging for skull base tumors.

MATERIALS AND METHODS: Fifty-nine patients with chondrosarcomas, chordomas, or metastases between January 2015 and October 2021 were included in this retrospective study. Pretreatment normalized mean ADC and dynamic contrast-enhanced MR imaging parameters were calculated. The Kruskal-Wallis H test for all tumor types and the Mann-Whitney *U* test for each pair of tumors were used.

RESULTS: Fifteen chondrosarcomas (9 men; median age, 62 years), 14 chordomas (6 men; median age, 47 years), and 30 metastases (11 men; median age, 61 years) were included in this study. Fractional plasma volume helped distinguish all 3 tumor types ($P = .003$, $<.001$, and $<.001$, respectively), whereas the normalized mean ADC was useful in distinguishing chondrosarcomas from chordomas and metastases ($P < .001$ and $P < .001$, respectively); fractional volume of extracellular space, in distinguishing chondrosarcomas from metastases ($P = .02$); and forward volume transfer constant, in distinguishing metastases from chondrosarcomas/chondroma ($P = .002$ and .002, respectively) using the Kruskal-Wallis H test. The diagnostic performances of fractional plasma volume for each pair of tumors showed areas under curve of 0.86–0.99 (95% CI, 0.70–1.0); the forward volume transfer constant differentiated metastases from chondrosarcomas/chordomas with areas under curve of 0.82 and 0.82 (95% CI, 0.67–0.98), respectively; and the normalized mean ADC distinguished chondrosarcomas from chordomas/metastases with areas under curve of 0.96 and 0.95 (95% CI, 0.88–1.0), respectively.

CONCLUSIONS: DWI and dynamic contrast-enhanced MR imaging sequences can be beneficial for differentiating the 3 common skull base tumors.

ABBREVIATIONS: AUC = area under the curve; DCE-MR imaging = dynamic contrast-enhanced perfusion MR imaging; IQR = interquartile range; K^{trans} = forward volume transfer constant; Ve = fractional volume of extracellular space; Vp = fractional plasma volume; nADCmean = normalized mean ADC

The skull base is involved in a wide variety of neoplasms.[1] They include primary bone tumors such as chondrosarcomas and chordomas, both of which show similarities in anatomic location, clinical manifestations, and conventional imaging findings, with a combined annual incidence of approximately 1 per 100,000.[2]

Received January 2, 2022; accepted after revision June 28.

From the Division of Neuroradiology (Y.O., E.L., A.A.C., A.B., R.K., M.K., A.S.), Department of Radiology, University of Michigan, Ann Arbor, Michigan; Department of Radiology (A.B.), Jikei University School of Medicine Ringgold Standard Institution, Tokyo, Japan; Department of Radiology (R.K.), The University of Tokyo Hospital, Tokyo, Japan; and Department of Radiology (M.K.), Tokyo Metropolitan Cancer and Infectious Diseases Center Komagome Hospital Ringgold Standard Institution, Bunkyo-ku, Japan.

Please address correspondence to Yoshiaki Ota, MD, University of Michigan, Department of Radiology, 1500 E Medical Center Dr, UH B2, Ann Arbor, MI 48109; e-mail: yoshiako@med.umich.edu; @GattsukiRadiol

http://dx.doi.org/10.3174/ajnr.A7607

Chondrosarcomas arise from the embryonic rest of the cartilaginous matrix of the cranium and tend to be centered at the petrous apex or petro-occipital fissure,[3] compared with chordomas that arise from remnants of the notochord and are typically centered on the clivus. However, both tumors tend to be locally aggressive, limiting the feasibility and diagnostic utility of establishing the site of origin on conventional CT and MR imaging.[4] In the skull base, especially in the clivus and petrous regions, skull base metastases are also diagnostic considerations. The prevalence of skull base metastases among patients with cancer remains to be revealed, but it has been suggested that it is underreported.[5] Breast, lung, prostate, and head and neck cancers, as well as melanomas have been reported.[6,7] Skull base metastases of unknown origin have been reported as well.[7] Conventional MR imaging has been reported as a sensitive tool to detect abnormalities in the skull base,[8] but MR imaging features are not specific and may overlap between chondrosarcomas and chondromas.[4] The

treatment strategy and long-term prognosis differ depending on the above-mentioned 3 tumors,[5,9] making it clinically important to distinguish them, especially in patients in whom an abnormality is detected on MR imaging or CT in the skull base but who do not have confirmed primary cancers elsewhere in the body.

DWI can characterize cellularity and unique microstructures, and dynamic contrast-enhanced MR imaging (DCE-MR imaging) can evaluate permeability patterns and vascularity[10-14] and is increasingly used for tumor differentiation and evaluation of treatment effects.[15,16] The ADC value has been shown to assist in the differentiation of chondrosarcomas and chordomas,[17] but the differentiation of metastases from chondrosarcomas and chordomas has not been fully explored. Recently, DCE-MR imaging has been used to differentiate bone metastases from benign lesions.[17,18] However, no studies have explored the differentiation of these 3 tumor types using DCE-MR imaging. The calculated parameters from DCE-MR imaging include fractional plasma volume (Vp), which can reflect tumor vascularity, as well as fractional volume of extracellular space (Ve) and forward volume transfer constant (K^{trans}), which can represent permeability.[11] Chondrosarcomas, chordomas, and metastases can show different internal structures, microvascularization, and permeability, suggesting that DWI and DCE-MR imaging can be helpful in the differentiation of the 3 tumor types.

In this study, we aimed to test the ability of DWI and DCE-MR imaging to differentiate chondrosarcomas, chordomas, and metastases in the skull base.

MATERIALS AND METHODS

Study Population

This retrospective single-center study was approved by University of Michigan institutional review board, and the requirement of informed consent was waived. Data were acquired and de-identified before any analysis, in compliance with all applicable Health Insurance Portability and Accountability Act regulations. We reviewed the medical records of 368 patients, including 68 patients diagnosed with chondrosarcomas, 60 patients with chordomas, and 240 patients with skull base metastases from January 2015 to October 2021 in a single center. Patients with chondrosarcomas and classic chondromas were diagnosed pathologically. Skull base metastases were diagnosed by biopsy or on the basis of the clinical evidence of confirmed primary cancers, other biopsied-confirmed metastatic lesions, and skull base lesions detected on conventional CT/MR imaging and FDG-PET/CT. Cases without pretreatment DWI or DCE-MR imaging (including biopsy, surgery, or radiation therapy) ($n = 295$) or poor image quality ($n = 14$) were excluded.

All 30 patients with skull base metastases had confirmed primary cancers. Six of 30 patients underwent a biopsy (3 lung cancers, 2 breast cancers, and 1 renal cell carcinoma), and 24 of 30 patients were clinically diagnosed on the basis of all 24 patients having histories of confirmed primary cancers, biopsy-confirmed metastatic lesions in the other regions, and positive conventional head and neck CT/MR imaging and PET/CT findings in the skull base. For patients diagnosed with skull base metastases, the treatment response of the skull base lesions following chemotherapy or chemotherapy plus radiation therapy was confirmed on follow-up CT or MR imaging. Corresponding treatments such as chemotherapy ($n = 18$) or chemotherapy plus radiation therapy ($n = 12$) were used, and a decrease in size was observed on CT or MR imaging.

In total, 59 patients (20 men, 39 women; median age, 61 years; interquartile range [IQR], 45–70 years) with 15 chondrosarcomas, 14 chordomas, and 30 skull base metastases were included in this study. Patient demographics such as age and sex for all tumor types and primary cancers for skull base metastases were reviewed from medical records.

MR Imaging Protocol

Head and neck MR imaging examinations were performed using a 1.5T or 3T system (Ingenia; Philips Healthcare) with patients in the supine position. The acquired sequences were axial plane T1WI, T2WI, FLAIR, and contrast-enhanced fat-saturated T1WI and coronal plane contrast-enhanced fat-saturated T1WI. DWI was performed using echo-planar imaging with the following DWI parameters: TE range, 58–106 ms; TR range, 5000–9500 ms; number of excitations, 1; section thickness and gap, 3.5–4 and 0–1 mm; FOV, 220–240 mm; matrix size, 128 × 128 to 200 × 200; and 3 diffusion directions. Sensitizing diffusion gradients were sequentially applied. B values were 0 and 1000 s/mm^2.

A DCE-MR imaging sequence was performed using a 3D T1-weighted fast-field echo technique with a 16-channel Neurovascular coil. Twenty milliliters of gadobenate dimeglumine (MultiHance; Bracco Diagnostics) was administered through a peripheral arm vein using a power injector at a flow rate of 5.0 mL/s and followed by a 20-mL saline flush. DCE-MR imaging was sequentially acquired with the following parameters of 3D-T1 fast-field echo: TE, 1.86 ms; TR, 4.6 ms; flip angle, 30°; section thickness, 5.0 mm; FOV, 240 × 240 mm^2; voxel size, 1.0 × 1.0 × 5.0 mm^3; number of excitations, 1; number of slices per dynamic scan, 48; temporal resolution, 8.4 seconds; dynamic phase, 30 dynamics; total acquisition time, 4 minutes 24 seconds.

Imaging Processing and Analysis

Two board-certified radiologists with 7 and 10 years of experience independently performed DWI and DCE-MR imaging analyses. The same board-certified radiologist with 7 years of experience reviewed conventional MR imaging. The 2 readers were blinded to the histologic results.

Conventional Imaging

The maximum axial diameter was measured using contrast-enhanced axial and coronal fat-saturated T1WI. As conventional MR imaging features, the main skull base location was identified using axial and coronal contrast-enhanced fat-saturated T1WI and recorded as the clivus or petrous bone. In addition, both radiologists evaluated the following imaging characteristics with consensus and recorded them as binary variables:

1) Cystic changes, defined as focal areas with nonenhancing, predominantly T2-hyperintense areas and necrotic changes defined as focal areas with nonenhancing, predominantly T1-hypointense and heterogeneously T2-hyperintense areas.
2) T2 hyperintensity or iso-/hypointensity in the lesion relative to the brain parenchyma, evaluated on T2WI, excluding the areas of cystic/necrotic changes.

Table 1: Patient demographics[a]

	Chondrosarcoma	Chordoma	Metastasis
No. of patients	15	14	30
Sex (male/total)	9/15	6/14	11/30
Age (yr)	62 (46–70)	47 (32–58)	61 (47–70)
Maximum axial diameter (mm)	29.5 (24–36)	33 (24–40)	18.5 (15–23)
Primary cancer type	NA	NA	11 Breast, 6 lung, 6 malignant melanoma, 4 head and neck, 2 sarcoma, 1 kidney

Note:—NA indicates not applicable.
[a] Values are presented as the median (IQR).

3) Enhancement patterns (homogeneous or heterogeneous), evaluated on postcontrast fat-saturated T1-weighted images.
4) Other metastatic lesions in the FOV of the head and neck scan, evaluated on T1WI, T2WI, and postcontrast T1WI.

DWI Analysis

The same 2 board-certified radiologists with 7 and 10 years of experience manually delineated a single freehand ROI on the axial contrast-enhanced fat-saturated T1WI. ADC maps were constructed using commercially available software (Olea Sphere, Version 3.0; Olea Medical). On the ADC maps, the corresponding ROIs were again contoured with reference to the ROIs delineated on axial postcontrast T1WI. The 2 readers adhered to the following procedure:

1) ROIs were encompassed in the areas on axial postcontrast fat-saturated T1WI where the tumors showed solid enhancing components, excluding necrotic or cystic regions. When the lesions extended beyond the clivus into surrounding soft tissues, both the bony and soft structures were included in a ROI.
2) The peripheral 2 mm of the lesions were excluded from an ROI to avoid volume averaging.
3) The ROIs were manually adjusted on the ADC map if geometric artifacts were observed.
4) An ROI was placed within the medulla oblongata as an internal control. The mean ADC values of the tumor were divided by the mean ADC values of the medulla oblongata, and the normalized mean ADC (nADCmean) was calculated.

DCE-MR Imaging Analysis

Quantitative analyses were performed using the Olea Sphere 3.0 software. An arterial input function was automatically computed. While this process was automated, the corresponding time-intensity curves that demonstrated a rapid increase in attenuation with sharp peaks were deemed appropriate and accurate for analysis. The permeability module was based on the extended Tofts model, and pixel-based parameter maps were calculated from time-intensity curves. ROIs were placed by means of the method used for the DWI analysis. Quantitative parameters, Vp, Ve, and K^{trans}, were calculated.

Statistical Analysis

nADCmean and Ve, K^{trans}, and Vp were compared among the 3 tumor types using the Kruskal-Wallis H test and the post hoc test with Bonferroni correction and were described as medians (IQR). The conventional MR imaging features were compared between each pair of tumor types by the Fisher exact test. For each pair of tumor type (chondrosarcomas and chordomas, chondrosarcomas and metastases, and chordomas and metastases), the parameters from DWI and DCE-MR imaging analyses were compared using the Mann-Whitney *U* test with a Bonferroni correction and described as median (IQR). For statistically significant diagnostic parameters, receiver operating characteristic analysis was performed with the optimal cutoff values, which were determined to maximize the Youden index (sensitivity + specificity-1). The intraclass correlation coefficient was used to assess the interobserver agreement for DWI and DCE-MR imaging parameters. All statistical calculations were conducted using R statistical and computing software (http://www.r-project.org/). Variables with P values $< .05$ were considered statistically significant.

RESULTS

Patient Demographics

There were 15 chondrosarcomas (9 men; median age, 62 years; IQR, 46–70 years), 14 chordomas (6 men; median age, 47 years; IQR, 32–58 years), and 30 metastases (11 men; median age, 61 years; IQR, 47–70 years) in this study. Patient demographic and tumor characteristics are summarized in Table 1. As shown in Table 1, the metastatic cohort was a heterogeneous group of primary cancer types. The 3 most frequently seen primary cancers were breast (37%, 11/30), lung (20%, 6/30), and malignant melanomas (20%, 6/30).

Conventional MR Imaging Features

The results of the comparisons between chondrosarcomas versus chordomas and between chondrosarcomas and chordomas versus metastases are presented in Table 2.

Chondrosarcomas versus Chordomas

There was no significant difference in main locations, the presence of cystic/necrotic changes, signal intensity (T2 hyperintensity or iso-/hypointensity), and enhancement patterns ($P = .08–1.0$).

Chondrosarcomas versus Metastases

T2 hyperintensity in the lesion was more often seen in chondrosarcomas than in metastases (10/15 versus 9/30, $P = .027$). Otherwise, there was no significant difference in main locations and the presence of cystic/necrotic changes or enhancement patterns between them ($P = .14–.29$).

Chordomas versus Metastases

T2 hyperintensity in the lesion was more often seen in chordomas than in metastases (9/14 versus 9/30; $P = .049$). Otherwise, there was no significant difference in other conventional imaging features between them ($P = .29–.65$).

Table 2: Conventional imaging characteristics of chondrosarcomas, chordomas, and metastases

	Chondrosarcoma	Chordoma	Metastasis	*P* Value
Main location (petrous bone:clivus)	9:6	1:13	5:25	$P^a = .08$ $P^b = .14$ $P^c = .65$
Cystic/necrotic changes	8/15	7/14	10/30	$P^a = 1.0$ $P^b = .22$ $P^c = .33$
T2 hyperintensity or iso-/hypointensity relative to the brain parenchyma (T2 hyperintensity/total)	10/15	9/14	9/30	$P^a = 1.0$ $P^b = .027$ $P^c = .049$
Enhancement patterns (heterogeneous/total)	15/15	14/14	26/30	$P^a = 1.0$ $P^b = .29$ $P^c = .29$
Other metastatic lesions in the head and neck	NA	NA	5/30	NA

Note:—P^a is obtained from a comparison between chondrosarcoma and chordoma, P^b is from a comparison between chondrosarcoma and metastasis, and P^c is from a comparison between chordoma versus metastasis.

Table 3: DWI and DCE-MR imaging parameters of chondrosarcoma, chordoma, and metastasis using the Kruskal-Wallis H test and the post hoc test with Bonferroni correction[a]

					P Value[b]		
	Chondrosarcoma	Chordoma	Metastasis	*P* Value[a]	Chondrosarcoma vs Chordoma	Chondrosarcoma vs Metastasis	Chordoma vs Metastasis
nADCmean	2.44 (2.27–2.71)	1.30 (1.07–1.73)	1.39 (1.21–1.70)	<.001	<.001	<.001	1.0
Vp	0.015 (0.01–0.028)	0.045 (0.04–0.068)	0.12 (0.09–0.14)	<.001	.003	<.001	<.001
Ve	0.25 (0.15–0.31)	0.35 (0.30–0.40)	0.48 (0.34–0.63)	.007	.14	.022	.17
K^{trans} (minute^{-1})	0.08 (0.06–0.17)	0.16 (0.13–0.20)	0.39 (0.20–0.63)	<.001	.16	.002	.002

Note:—P^a is from Kruskal–Wallis H test. P^b is adjusted for pair-wise comparison by Bonferroni correction.
[a] Numbers in parentheses indicate interquartile range.

DWI and DCE-MR Imaging Analysis

The intraclass correlation coefficient for DWI and DCE-MR imaging parameters was excellent (nADCmean, 0.94; Vp, 0.95; K^{trans}, 0.97; Ve, 0.95).

In the Kruskal-Wallis H test and the post hoc test with a Bonferroni correction, there were statistically significant differences in nADCmean, Vp, Ve, and K^{trans} among all tumor types (nADCmean, $P < .001$; Vp, $P < .001$; Ve, $P = .007$; and K^{trans}, $P < .001$). Vp showed significant differences in each pair of tumors (chondrosarcomas versus chordomas, $P = .003$; chondrosarcomas versus metastases, $P < .001$; and chordomas versus metastases, $P < .001$, respectively). Table 3 and Fig 1 summarize the comparisons of DWI and DCE-MR imaging parameters among the 3 tumors.

Chondrosarcomas versus Chordomas

The median nADCmean was significantly higher and the median Vp was significantly lower in chondrosarcomas than in chordomas (nADCmean: 2.4 [IQR, 2.3–2.7] versus 1.30 [IQR, 1.07–1.73; $P < .001$; Vp: 0.015 [IQR, 0.01–0.028] versus 0.045 [IQR, 0.04–0.068]; $P = .012$), while the median Ve and K^{trans} were insignificantly different (Ve: 0.25 [IQR, 0.15–0.31] versus 0.35 [IQR, 0.30–0.40]; $P = .57$; K^{trans}: 0.08 [IQR, 0.06–0.17] versus 0.16 [IQR, 0.13–0.20]; $P = .64$).

Chondrosarcomas versus Metastases

nADCmeans were significantly higher, and Vp and K^{trans} were significantly lower in chondrosarcomas than in metastases (nADCmean: 2.44 [IQR, 2.27–2.71] versus 1.39 [IQR, 1.21–1.70]; $P < .001$; Vp: 0.015 [IQR, 0.01–0.028] versus 0.12 [IQR, 0.09–0.14]; $P < .001$; K^{trans}: 0.08 [IQR, 0.06–0.17] versus 0.39 [IQR, 0.20–0.63]; $P = .008$), while Ve was insignificantly different (Ve: 0.25 [IQR, 0.15–0.31] versus 0.48 [IQR, 0.34–0.63]; $P = .09$).

Chordomas versus Metastases

Median Vp and K^{trans} were significantly lower in chordomas than in metastases (Vp: 0.045 [IQR, 0.04–0.068] versus 0.12 [IQR, 0.09–0.14]; $P < .001$; K^{trans}: 0.16 [IQR, 0.13–0.20] versus 0.39 [IQR, 0.20–0.63]; $P = .008$), while nADCmean and Ve were insignificantly different (nADCmean: 1.30 [IQR, 1.07–1.73] versus 1.39 [IQR, 1.21–1.70]; $P = 1.0$; Ve: 0.35 [IQR, 0.30–0.4] versus 0.48 [IQR, 0.34–0.63]; $P = .68$).

Diagnostic Performance of DWI and DCE-MR Imaging

The diagnostic performance of parameters of DWI and DCE-MR imaging analyses, which showed significant differences between chondrosarcomas versus chordomas, chondrosarcomas versus metastases, and chordomas versus metastases is demonstrated in Table 4 and Fig 2.

nADCmean showed areas under the curve (AUCs) of 0.96 and 0.95 (95% CI, 0.88–1.0) between chondrosarcomas and chordomas and between chondrosarcomas and metastases, respectively. Vp showed AUCs of 0.86, 0.99, and 0.92 (95% CI, 0.72–1.0) between chondrosarcomas and chordomas, between chondrosarcomas and metastases, and between chordomas and metastases, respectively. K^{trans} showed AUCs of 0.82 and 0.82 (95% CI, 0.67–0.98) between chondrosarcomas and metastases and between chordomas and metastases, respectively.

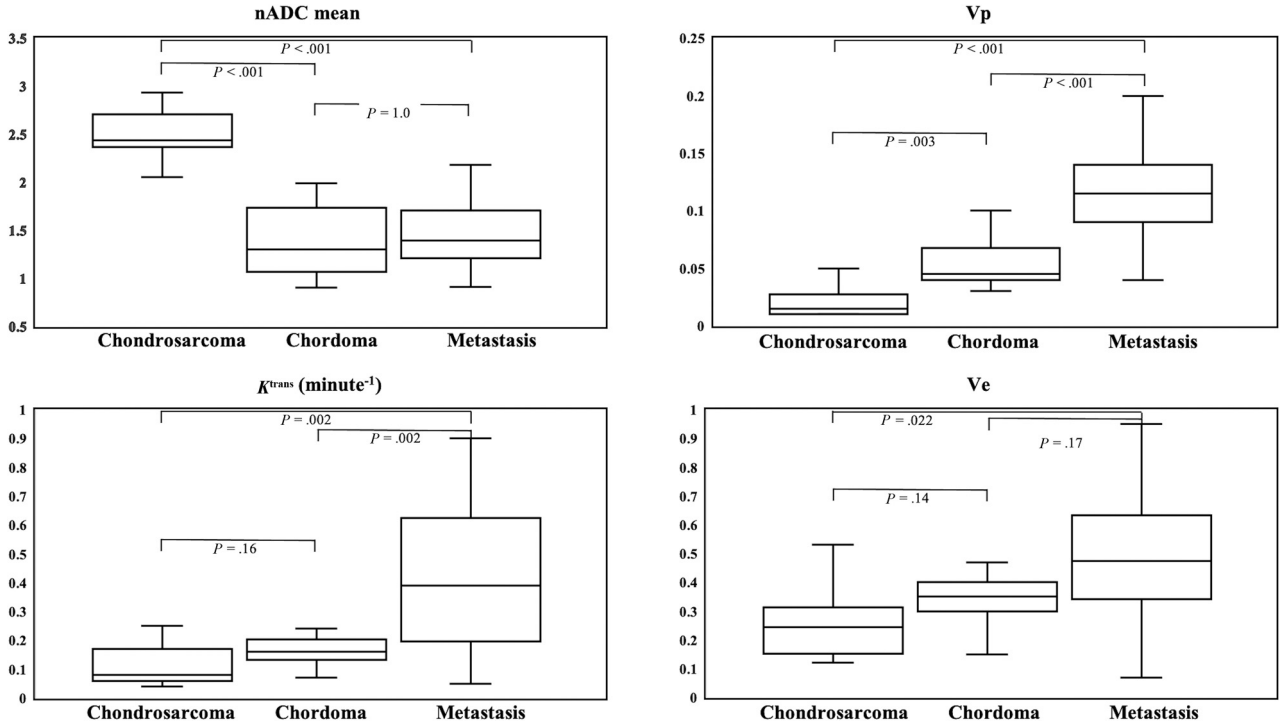

FIG 1. Box-and-whisker plots of DWI and DCE-MR imaging parameters with the Kruskal-Wallis H test and post hoc test with the Bonferroni correction are shown. The *boundaries* of boxes represent 25th and 75th percentiles, and the *lines* in boxes indicate medians.

Table 4: Diagnostic performance of DCE-MR imaging parameters for each tumor comparison[a]

	Chondrosarcoma vs Chordoma		Chondrosarcoma vs Metastasis			Chordoma vs Metastasis	
Parameters	nADCmean	Vp	nADCmean	Vp	K^{trans} (minute^{-1})	Vp	K^{trans} (minute^{-1})
Cutoff	1.99	0.03	2.09	0.06	0.12	0.09	0.30
Sensitivity	1.0 (0.68–1)	0.93 (0.66–0.99)	0.93 (0.76–0.99)	0.93 (0.78–0.99)	0.93 (0.78–0.99)	0.80 (0.61–0.92)	0.60 (0.41–0.77)
Specificity	0.86 (0.57–0.98)	0.71 (0.42–0.92)	0.87 (0.60–0.98)	0.93 (0.66–0.9)	0.71 (0.42–0.92)	0.93 (0.66–1)	1.0 (0.68–1)
PPV	0.88 (0.62–0.98)	0.77 (0.50–0.93)	0.93 (0.76–0.99)	0.97 (0.82–1)	0.88 (0.71–0.97)	0.96 (0.80–1)	1.0 (0.74–1)
NPV	1.0 (0.64–1)	0.91 (0.59–0.99)	0.87 (0.60–0.98)	0.87 (0.60–0.98)	0.83 (0.52–0.98)	0.68 (0.43–0.87)	0.54 (0.33–0.73)
Accuracy	0.93 (0.78–0.99)	0.82 (0.63–0.94)	0.91 (0.77–0.97)	0.93 (0.81–0.99)	0.86 (0.73–0.95)	0.84 (0.70–0.93)	0.73 (0.57–0.85)
AUC	0.96 (0.90–1)	0.86 (0.72–1)	0.95 (0.88–1)	0.99 (0.96–1)	0.82 (0.67–0.98)	0.92 (0.84– 1)	0.82 (0.70–0.95)

Note:—PPV indicates positive predictive value; NPV, negative predictive value.
[a] Numbers in parentheses represent 95% CIs.

Representative cases of chondrosarcoma, chordoma, and metastasis with DWI and DCE-MR imaging analyses are shown in Figs 3–5.

DISCUSSION

This study aimed to test the utility of DWI and DCE-MR imaging for skull base chondrosarcomas, chordomas, and metastases. nADCmean, Vp, Ve, and K^{trans} showed significant differences among all tumor types, and Vp showed significant differences between each pair of tumor comparisons using the Kruskal-Wallis H test. In the Mann-Whitney *U* test for each pair of 2 tumors, Vp distinguished all tumor types with AUCs of 0.86–0.99 with cutoffs of 0.03–0.09, K^{trans} distinguished metastases from chondrosarcomas and chordomas with an AUC of 0.82 with cutoffs of 0.12 and 0.30, and nADCmean distinguished chondrosarcomas from chordomas and metastases with AUCs of 0.96 and 0.95 and cutoffs of 1.99 and 2.09, respectively. Ve was not a significant differentiator of tumor types.

Regarding conventional MR imaging features, T2 hyperintensity of the lesion was shown to be significantly higher in chondrosarcomas and chordomas than in metastases, which can be used as a differentiator from metastases between chondrosarcomas and chordomas. Other imaging features such as main locations, cystic/necrotic changes, or enhancement patterns did not identify any significant difference between each pair of tumor type. Also, in patients with metastases, only 5 of 30 patients showed other metastatic lesions in head and neck MR imaging, suggesting that other metastatic lesions may not be a decisive factor for differentiation of these tumors.

Regarding DWI analysis, ADC values were lower in chordomas than in chondrosarcomas in this study, as suggested by a previous study.[17] It has been suggested that the difference in tumoral microstructure, such as cartilaginous stroma with varying degrees of cellularity in chondrosarcomas as well as myxoid stroma arranged through sheets of physaliferous cells in chordoma, contributes to the difference in ADC values.[17] ADC values were also lower in metastases than in chondrosarcomas. Generally, malignant tumors show

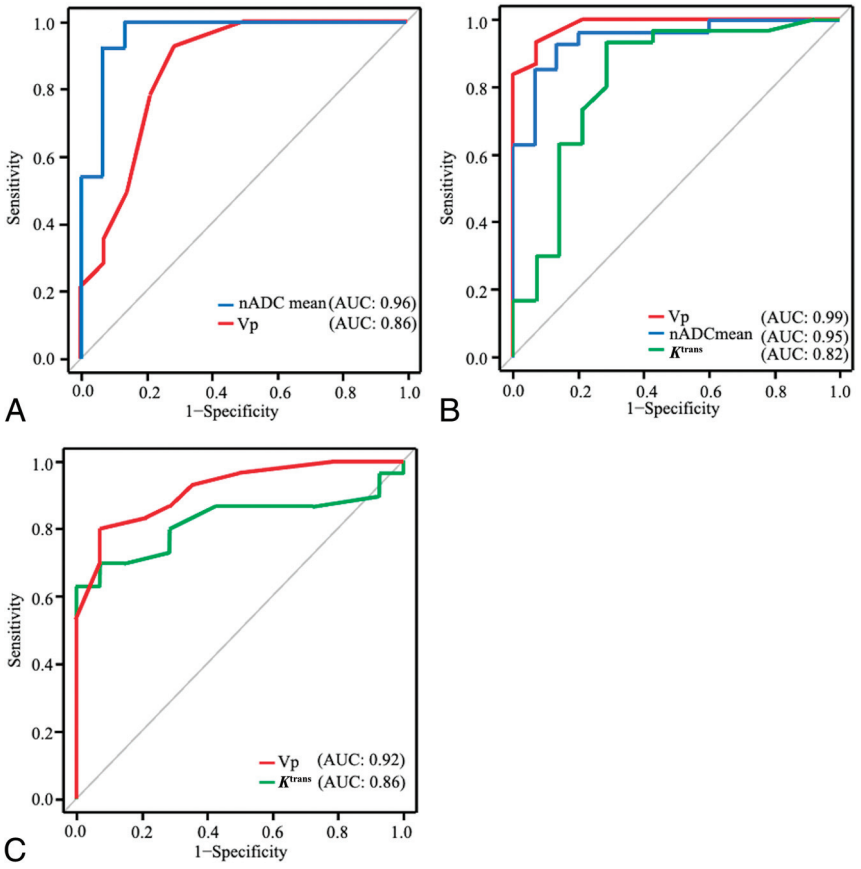

FIG 2. Receiver operating characteristic curves of chondrosarcoma versus chordoma (*A*), chondrosarcoma versus metastasis (*B*), and chordoma versus metastasis (*C*) are shown.

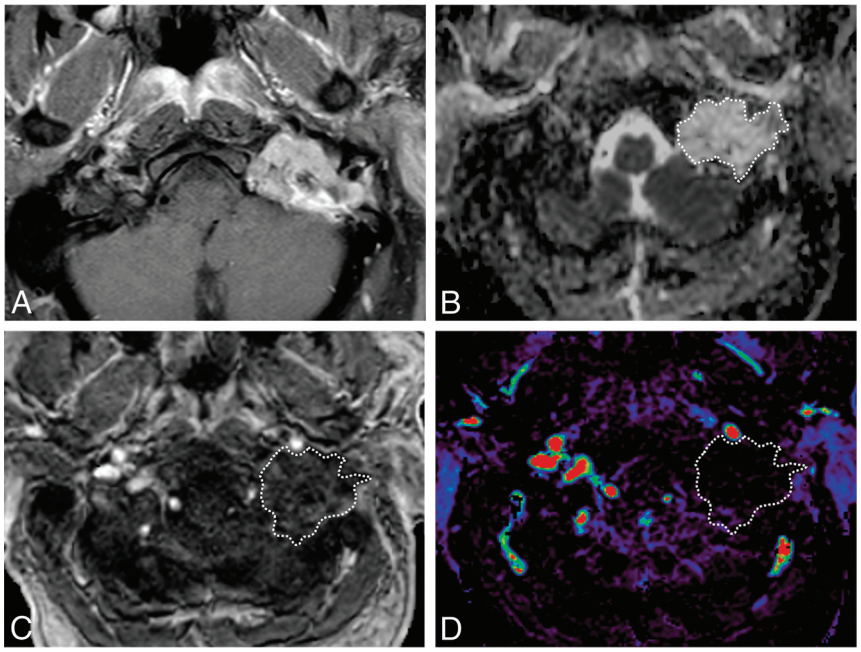

FIG 3. A 56-year-old man with a chondrosarcoma in the left petrous apex. *A*, Axial fat-saturated postcontrast T1-weighted image shows a heterogeneously enhancing mass in the left petrous apex. *B*, An ROI was placed on the ADC map, and the nADCmean was calculated. Mean ADC and ADC values in the medulla were 2.05, and 0.80 $\times$ 10^{-3} mm^2/s, respectively. The nADCmean was 2.56. *C*, An ROI was placed on the permeability map, and Vp, K^{trans}, and Ve were calculated. *D*, Vp is 0.01.

high cellularity, which is assumed to result in low ADC values in metastases.[19] In contrast, nADCmean was not a significant differentiator between chordomas and metastases, which is thought to stem from the complexity of internal structures and cellularity of each tumor group or from the heterogeneity of primary cancers of metastases. We divided the ADC values of the tumors by those of the medulla oblongata for normalization to minimize variations due to differences in magnetic field and scanner parameters. The medulla is usually included within the FOV of head and neck protocols and is rarely affected by chronic microvascular diseases,[20] offering easy reproducibility of the internal standard reference. This standardization method was thought to make our results robust.

Regarding DCE-MR imaging analysis, Vp, which is a marker of microvascularity, was lowest in chondrosarcomas, intermediate in chordomas, and highest in metastases, with significant differences, and showed promising diagnostic performances in the receiver operating characteristic analysis. Both chondrosarcomas and chordomas are known to have poor vascularity,[21-23] and DCE-MR imaging has been used to investigate each tumor type separately.[24,25] However, there have been no studies that compared perfusion characteristics between chondrosarcomas and chordomas using DCE-MR imaging perfusion. On the basis of our study, Vp and ADC values can be significant differentiators between the 2 tumors, with promising diagnostic performance. In addition, clival metastases, which included a variety of primary cancer types such as breast, lung, melanoma, and head and neck cancers, showed significantly higher Vp values than chondrosarcomas and chordomas. Previous studies have shown that there were no significant differences in Vp between vertebral hematologic malignancies and solid malignancy metastases[18] or between breast and lung cancer metastases.[26] However, a study showed higher Vp in vertebral metastasis from renal cancer (known as a hypervascular tumor) than from prostate cancer metastases (known as a hypovascular tumor).[27] This finding suggests that Vp in bone metastases can vary according to the primary cancer type. Nevertheless, when

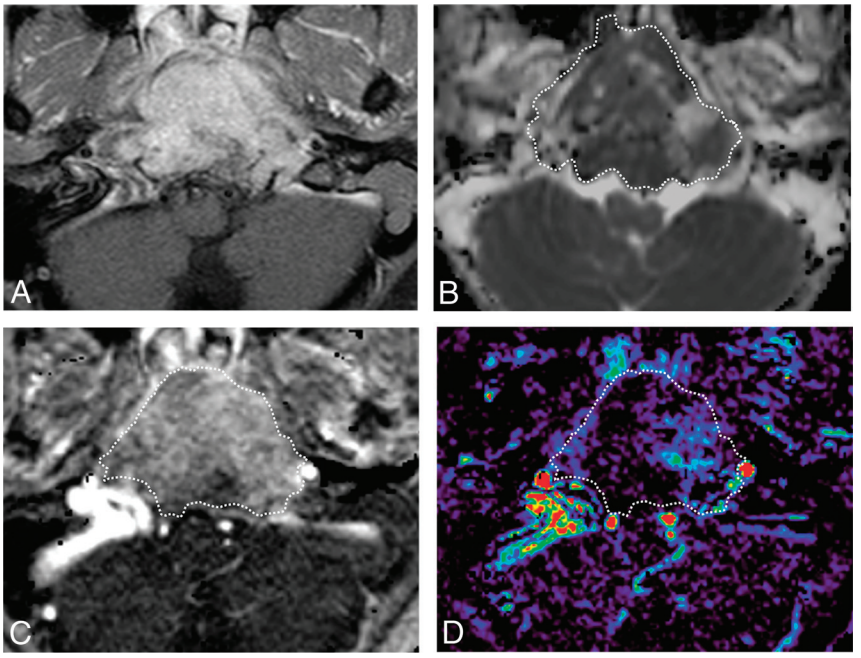

FIG 4. A 16-year-old boy with a chordoma in the clivus. *A*, Axial fat-saturated postcontrast T1-weighted image shows a heterogeneously enhancing mass in the clivus. *B*, An ROI was placed on the ADC map, and the nADCmean was 1.5. *C*, An ROI was placed on the permeability map, and Vp, K^{trans}, and Ve were calculated. *D*, Vp is 0.08.

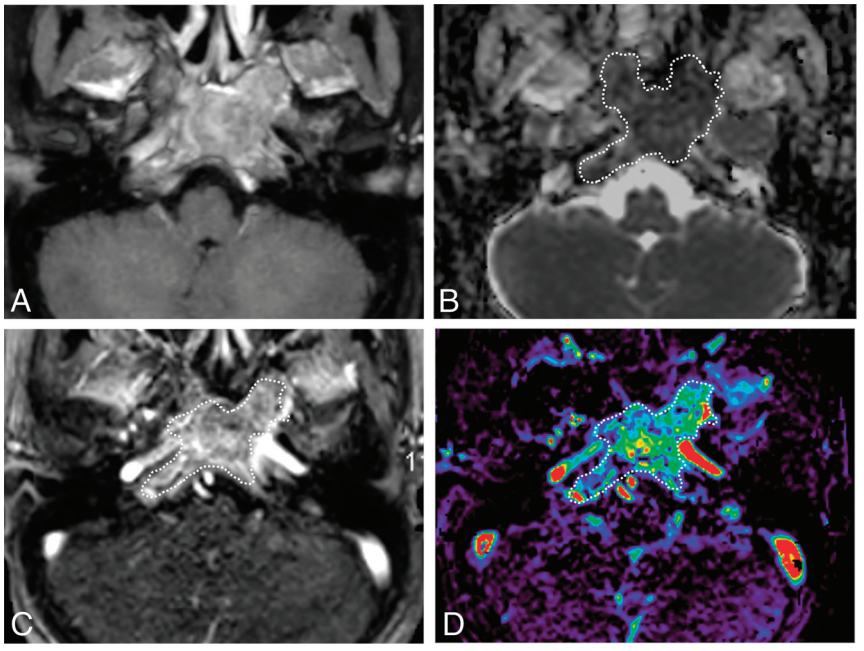

FIG 5. A 39-year-old woman with a metastatic breast cancer lesion in the clivus. *A*, Axial fat-saturated postcontrast T1-weighted image shows a heterogeneously enhancing mass in the clivus. *B*, An ROI was placed on the ADC map, and the nADCmean was 0.97. *C*, An ROI was placed on the permeability map, and Vp, K^{trans}, and Ve were calculated. *D*, Vp showed 0.23.

metastatic lesions are grouped together as a general population, irrespective of the primary cancer type, our results suggest that Vp remains a significant differentiator from primary bone lesions, such as chordomas or chondrosarcomas.

K^{trans}, which is a marker of tumor permeability, was higher in metastases than in the chondrosarcomas and chordomas in our study. Malignant tumors generally show higher tumor permeability than benign tumors.[26] Similar to Vp, K^{trans} within the metastatic cohort can demonstrate variation on the basis of the type of primary malignancy,[27] though our overall results suggest that the general population of metastatic lesions will demonstrate significantly higher K^{trans} than primary bone lesions such as chordomas or chondrosarcomas. There were no significant differences in K^{trans} between chondrosarcomas and chordomas; therefore, it was not applicable for the differentiation of the 2 tumors on the basis of our results.

In our study, nADCmean showed the highest diagnostic performance in differentiating chondrosarcomas from chordomas, while Vp distinguished skull base metastases from chondrosarcomas and chordomas with the highest diagnostic performance. A biopsy is typically required for definite diagnosis and management. However, there are some clinical situations in which the invasive diagnostic procedure could be avoided. In fact, avoiding a biopsy in favor of short-term follow-up scans is often recommended at multidisciplinary conferences when the lesions are located close to or involve the vasculature or when the patients tend to have comorbidities that put them at higher risk of hemorrhage. In these clinical settings, adding DWI and DCE-MR imaging can be beneficial for clinical judgment and further management. In addition, when conventional imaging is indeterminate or PET/CT is not available or feasible at the time of diagnosis, DWI and DCE-MR imaging can enhance the confidence in the diagnosis when combined with the conventional imaging findings and can assist in proper clinical management.

There were several limitations to this study. First, it was retrospectively conducted at a single institution and included a relatively small population. In addition, we could not include head and neck CT imaging features because head and neck CT was not performed in all included patients. Second, most metastases ($n = 24$) could not be histologically confirmed owing to the anatomic accessibility of the skull base and risk of complications. However, all cases had confirmed primary cancers with abnormal skull base findings on CT or MR imaging and PET/CT, and other metastatic lesions were detected by biopsy or surgery. Third, this study used 1.5T and 3T scanners, which might result

in heterogeneity of DCE-MR imaging parameters. Forth, we did not conduct out-of-sample validation in statistical analysis, which potentially caused overly optimistic results in the diagnostic performance of DWI and DCE-MR imaging parameters. Finally, we included heterogeneous primary cancer diseases in patients with metastases, though this heterogeneous group can represent general populations of patients with cancer.

CONCLUSIONS

DWI and DCE-MR imaging sequences can help differentiate chondrosarcomas, chordomas, and metastases. When a skull base lesion is indeterminate on conventional imaging and/or a biopsy should be avoided due to the location of the lesion in close proximity to major vasculature or the patient's underlying comorbidities, DWI and DCE-MR imaging sequences can enhance the confidence in arriving at an appropriate diagnosis.

Disclosure forms provided by the authors are available with the full text and PDF of this article at www.ajnr.org.

REFERENCES

1. Kelly HR, Curtin HD. **Imaging of skull base lesions.** *Handb Clin Neurol* 2016;135:637–57 CrossRef Medline
2. Dolecek TA, Propp JM, Stroup NE, et al. **CBTRUS statistical report: primary brain and central nervous system tumors diagnosed in the United States in 2005-2009.** *Neuro Oncol* 2012;1(Suppl 5):v1–49 CrossRef Medline
3. Almefty K, Pravdenkova S, Colli BO, et al. **Chordoma and chondrosarcoma: similar, but quite different, skull base tumors.** *Cancer* 2007;110:2467–67 CrossRef Medline
4. Pamir MN, Ozduman K. **Analysis of radiological features relative to histopathology in 42 skull-base chordomas and chondrosarcomas.** *Eur J Radiol* 2006;58:461–70 CrossRef Medline
5. Mehta GU, Raza SM. **Management of skull base metastases.** *Neurosurg Clin N Am* 2020;31:659–66 CrossRef Medline
6. Chaichana KL, Flores M, Acharya S, et al. **Survival and recurrence for patients undergoing surgery of skull base intracranial metastases.** *J Neurol Surg B Skull Base* 2013;74:228–35 CrossRef Medline
7. Laigle-Donadey F, Taillibert S, Martin-Duverneuil N, et al. **Skull-base metastases.** *J Neurooncol* 2005;75:63–69 CrossRef Medline
8. Mitsuya K, Nakasu Y, Horiguchi S, et al. **Metastatic skull tumors: MRI features and a new conventional classification.** *J Neurooncol* 2011;104:239–45 CrossRef Medline
9. Kremenevski N, Schlaffer SM, Coras R, et al. **Skull base chordomas and chondrosarcomas.** *Neuroendocrinology* 2020;110:836–47 CrossRef Medline
10. Surov A, Meyer HJ, Wienke A. **Apparent diffusion coefficient for distinguishing between malignant and benign lesions in the head and neck region: a systematic review and meta-analysis.** *Front Oncol* 2019;9:1362 CrossRef Medline
11. Gaddikeri S, Gaddikeri RS, Tailor T, et al. **Dynamic contrast-enhanced MR imaging in head and neck cancer: techniques and clinical applications.** *AJNR Am J Neuroradiol* 2016;37:588–95 CrossRef Medline
12. Ota Y, Moore AG, Spector ME, et al. **Prediction of wound failure in patients with head and neck cancer treated with free flap reconstruction: utility of CT perfusion and MR perfusion in the early postoperative period.** *AJNR Am J Neuroradiol* 2022;43:585–91 CrossRef Medline
13. Ota Y, Liao E, Capizzano AA, et al. **MR diffusion and dynamic-contrast enhanced imaging to distinguish meningioma, paraganglioma, and schwannoma in the cerebellopontine angle and jugular foramen.** *J Neuroimaging* 2021;32:502–10 CrossRef Medline
14. Ota Y, Naganawa S, Kurokawa R, et al. **Assessment of MR imaging and CT in differentiating hereditary and nonhereditary paragangliomas.** *AJNR Am J Neuroradiol* 2021;42:1320–26 CrossRef Medline
15. Ota Y, Liao E, Capizzano AA, et al. **Diagnostic role of diffusion-weighted and dynamic contrast-enhanced perfusion MR imaging in paragangliomas and schwannomas in the head and neck.** *AJNR Am J Neuroradiol* 2021;42:1839–46 CrossRef Medline
16. Ota Y, Liao E, Kurokawa R, et al. **Diffusion-weighted and dynamic contrast-enhanced MRI to assess radiation therapy response for head and neck paragangliomas.** *J Neuroimaging* 2021;31:1035–43 CrossRef Medline
17. Yeom KW, Lober RM, Mobley BC, et al. **Diffusion-weighted MRI: distinction of skull base chordoma from chondrosarcoma.** *AJNR Am J Neuroradiol* 2013;34:1056–61, S1 CrossRef Medline
18. Guan Y, Peck KK, Lyo J, et al. **T1-weighted dynamic contrast-enhanced MRI to differentiate nonneoplastic and malignant vertebral body lesions in the spine.** *Radiology* 2020;297:382–89 CrossRef Medline
19. Ginat DT, Mangla R, Yeaney G, et al. **Diffusion-weighted imaging for differentiating benign from malignant skull lesions and correlation with cell density.** *AJR Am J Roentgenol* 2012;198:W597–601 CrossRef Medline
20. Koontz NA, Wiggins RH 3rd. **Differentiation of benign and malignant head and neck lesions with diffusion tensor imaging and DWI.** *AJR Am J Roentgenol* 2017;208:1110–15 CrossRef Medline
21. Katonis P, Alpantaki K, Michail K, et al. **Spinal chondrosarcoma: a review.** *Sarcoma* 2011;2011:378957 CrossRef Medline
22. Fromm J, Klein A, Baur-Melnyk A, et al. **Survival and prognostic factors in conventional central chondrosarcoma.** *BMC Cancer* 2018;18:849 CrossRef Medline
23. Bergh P, Kindblom LG, Gunterberg B, et al. **Prognostic factors in chordoma of the sacrum and mobile spine: a study of 39 patients.** *Cancer* 2000;88:2122–34 CrossRef Medline
24. Santos P, Peck KK, Arevalo-Perez J, et al. **T1-weighted dynamic contrast-enhanced MR perfusion imaging characterizes tumor response to radiation therapy in chordoma.** *AJNR Am J Neuroradiol* 2017;38:2210–16 CrossRef Medline
25. De Coninck T, Jans L, Sys G, et al. **Dynamic contrast-enhanced MR imaging for differentiation between enchondroma and chondrosarcoma.** *Eur Radiol* 2013;23:3140–52 CrossRef Medline
26. Morales KA, Arevalo-Perez J, Peck KK, et al. **Differentiating atypical hemangiomas and metastatic vertebral lesions: the role of T1-weighted dynamic contrast-enhanced MRI.** *AJNR Am J Neuroradiol* 2018;39:968–73 CrossRef Medline
27. Saha A, Peck KK, Lis E, et al. **Magnetic resonance perfusion characteristics of hypervascular renal and hypovascular prostate spinal metastases: clinical utilities and implications.** *Spine (Phila Pa 1976)* 2014;39:E1433–40 CrossRef Medline